# Modelling and testing of a non-standard scanning device with dose reduction potential

Hugo de las Heras<sup>a</sup>, Oleg Tischenko<sup>a</sup>, Werner Panzer<sup>a</sup>, Yuan Xu<sup>b</sup> and Christoph Hoeschen<sup>a</sup>

GSF National Research Center for Environment and Health Ingolstaedter Landstrasse, 1

D-85764 Neuherberg, Germany;

<sup>b</sup>Department of Mathematics, University of Oregon Eugene, OR 97403-1222.

#### ABSTRACT

A non-standard scanning device with dose-reduction potential was proposed at the SPIE Medical Imaging conference 2006. The new device obtains the Radon data after the X-ray beam is collimated through a special mask. This mask is combined with a new geometry that permits an efficient data collection, thus the device has the potential of reducing the dose by a factor of two. In this work, we report a prototype of the new device and experimental data acquisition using only the mask of the new scanning geometry. In order to obtain the optimal parameters for the scanning device, several factors have been considered, including detector elements and shielding shape, fan beam angle, speed of the source rotation and materials employed. The calibration of the detector elements needs especial attention, due to the dependence of the detector response on the energy of the X-rays. A simplified version of the device was designed and mounted. Phantom data were acquired using this prototype and were used to test the performance of the new design. The results obtained are highly promising, even though the prototype developed does not make use yet of all the potential features proposed in the theory.

**Keywords:** CT, reconstruction, scanning geometry, scanning device

# 1. INTRODUCTION

The amount of X-ray radiation currently applied in CT practice is not utilized optimally<sup>1</sup>. A portion of radiation traversing the patient is either not detected at all or is used ineffectively<sup>2,3</sup>. The reason lies partly in the reconstruction algorithms<sup>4</sup> and partly in the geometry of the CT scanners designed specifically for these algorithms. In fact, the reconstruction methods widely used in CT are intended to invert the data that correspond to ideal straight lines<sup>5</sup>. However, the collection of such data is often not accurate due to likely movement of the source/detector system of the scanner during two succesive read-outs. In a paper presented in the conference SPIE Medical Imaging 2006<sup>6</sup>, a new design of the scanner geometry was proposed that is immune to the movement of the CT system and collects all radiation traversing the patient, thus having the potential of reducing the patient dose by a factor of two. Furthermore, the data acquired can be used by the FBP reconstruction algorithm and it is particularly suitable for OPED, an alternative algorithm based on expansion in polynomial series<sup>7,8</sup>.

The idea of the new scanner is recalled in Fig. 1 from Ref. 6. A collimating mask, fixed with the object, is placed between the source and the usual detector set. This collimating mask has detectors in its inner part and therefore enables all X-rays traversing the object to be collected. At the same time, the collection of data is inmune to unwanted movements of the X-ray source, which means that the collected data correspond precisely to the straight lines required by the reconstruction methods.

This paper deals with the first experiment of data acquisition that make use of this ideal geometry. In this first study, we focus on testing the idea of collimating mask, leaving the outter detectors for future analysis. A ring of detectors has been designed, built and tested with a real phantom. The source was kept still and the ring of detectors together with the phantom was rotated. The main goal of the work is to obtain an experimental verification of the idea explained in the previous papers of the last SPIE Medical Imaging Conference (Refs. 6 and 8).

Send correspondence to Hugo de las Heras E-mail: hugo.heras@gsf.de, Telephone: +49 89 3187 3773

Medical Imaging 2007: Physics of Medical Imaging, edited by Jiang Hsieh, Michael J. Flynn, Proc. of SPIE Vol. 6510, 65103R, (2007) · 1605-7422/07/\$18 · doi: 10.1117/12.705803

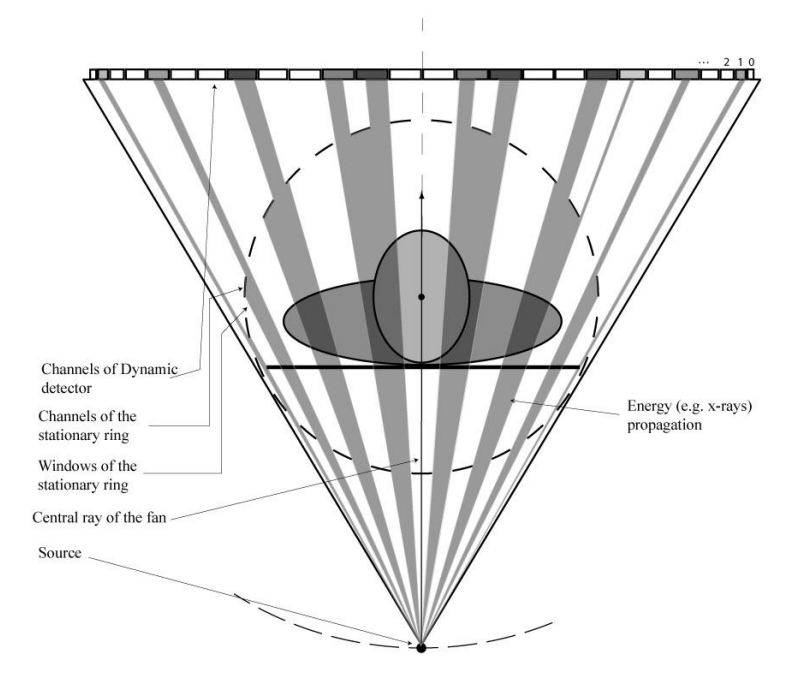


Figure 1. The idea of the new scanning geometry presented in the Conference SPIE Medical Imaging 2006<sup>6</sup>.

#### 2. METHODS

This section describes various parts of the new device, as well as the mount process and the test measurements.

# 2.1. The Detector Elements and Their Calibration

The detector elements are based on a CsI scintillator crystal of  $1 mm^2$  covered by a reflecting coating of  $TiO_2$  to improve light capture efficiency and connected to an optic fibre (Radcal Corp. Monrovia, California). The assemble ends up in a photo-diode that collects the light for a time to be chosen (Scanditronix-Wellhöfer, Schwarzenbruck, Germany). A total of 197 detector elements are used for the experiment.

In order to calibrate the detectors, they were irradiated in sets of 18 detectors at a distance of 169 cm from the source (see Fig. 2). The size and the homogeneity of the irradiation field was checked with a fluorescent screen while wearing lead protection. The dose at that distance was measured with a ionization chamber M23361 - 290 (Physikalisch-Technische Bundesanstalt PTB, Braunschweig), whose calibration was as well tested using a radioactive check source of  $Sr^{90}/Y^{90}$  and an Unidos dosemeter (PTW, Freiburg, Germany) also calibrated.

The detector response was obtained for different input-energies and different dose rates (see Table 1).

Table 1. The parameters employed in the calibration of the detectors

kilovoltage (kV)	Current (mA)	Filter (mm Al)		
50	3.75, 5, 7.5, 10, 12.5, 15	4.05		
70	3.75, 5, 7.5, 10, 12.5, 15	4.05		
90	3.75, 5, 7.5, 10, 12.5, 15	4.05		
110	3.75, 5, 7.5, 10, 12.5, 15	4.05		

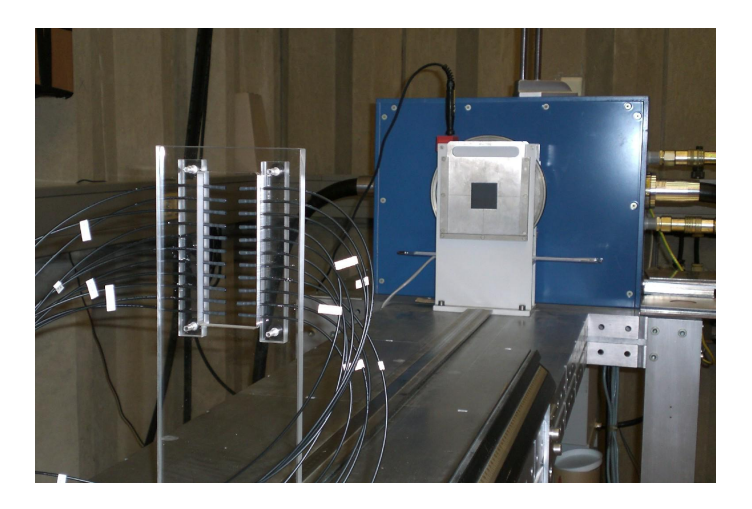


Figure 2. The set-up for the detector calibration.

A calibration factor can be obtained for every detector and every energy as the proportionality relation between dose and detector measurement (the slopes  $S_{50}$ ,  $S_{70}$ ,  $S_{90}$  and  $S_{110}$  of each curve in Fig. 10). This calibration can be used to estimate the dose in  $\mu Gy$  from the detector readings at a given radiation energy. Nevertheless, we can also obtain a correction factor by defining

$$F_{50,i} = \frac{S_{50,i}}{\overline{S_{50}}},\tag{1}$$

where

$$\overline{S_{50}} = \frac{\sum_{i=1}^{198} S_{50,i}}{108}.$$
 (2)

The factors  $F_{50,i}$ ,  $F_{70,i}$ ,  $F_{90,i}$  and  $F_{110,i}$  are only slightly energy dependent. They cannot be used to estimate the dose anymore, but they take into account the relative relation among the detectors, which is the information required to carry out a correct reconstruction. For the detector number i, the final factor that will correct its reading is given by

$$F_{i} = \frac{1}{4} \left( F_{50,i} + F_{70,i} + F_{90,i} + F_{110,i} \right). \tag{3}$$

An example of this process for the first 5 detectors is given in table 2 in the results section.

#### 2.2. Other Characteristics of the Scanner Device

The device basis is a PMMA "Plexiglas" ring with 197 holes for the detectors and their shielding. The distance from the detector to the centre of the device is 25 cm. The design details are shown in Figs. 3 and 4.

The lead pieces of shielding were made by pressing thin stripes of lead inside a press-form constructed especially for this case (Fig. 5).

The pressed stripes of the desired form were then cut into pieces of 1.8 cm. The shields were glued to the detectors using silicon, and the two together were stuck in the holes using a stronger type of silicon. In the latter step, the detectors and their shields are fixed to enable a rotation of the device, but they can also be taken out after the measurements and installed again in an optimised device. An image of the device under construction is shown in Fig. 6.

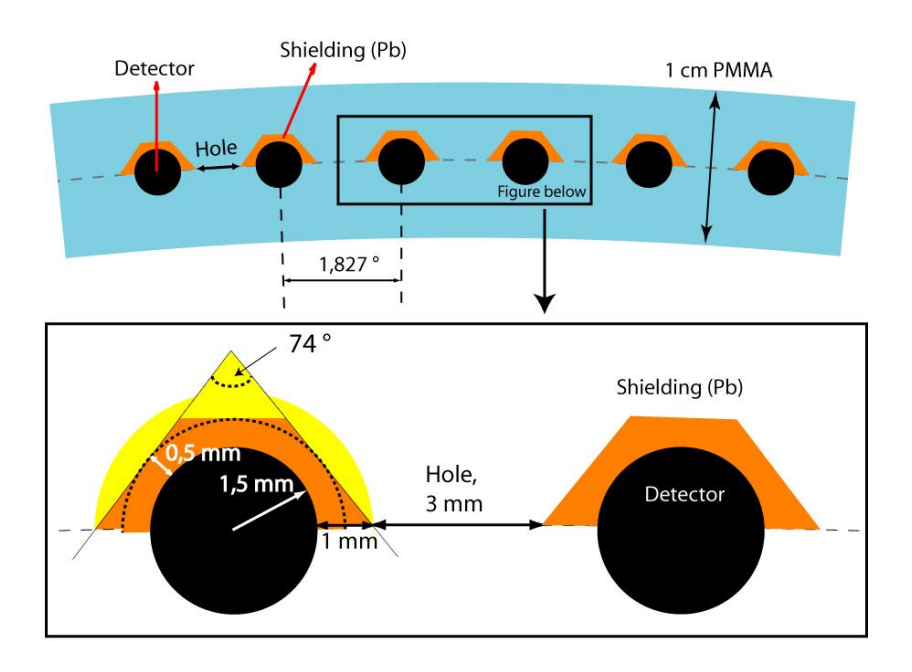


Figure 3. The structure of the ring and a detailed portion of two detectors.

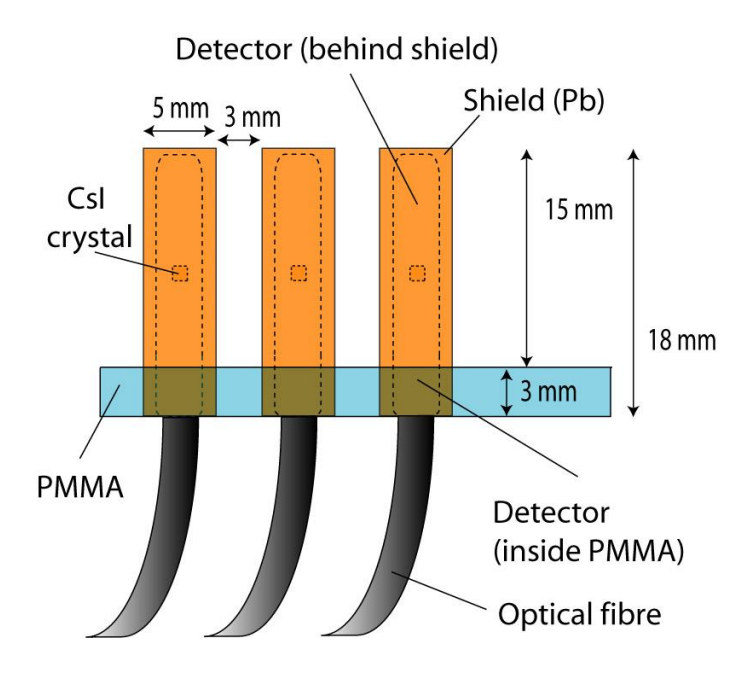


Figure 4. Lateral view of the device



Figure 5. The lead stripes and the pressing form for obtaining the shields

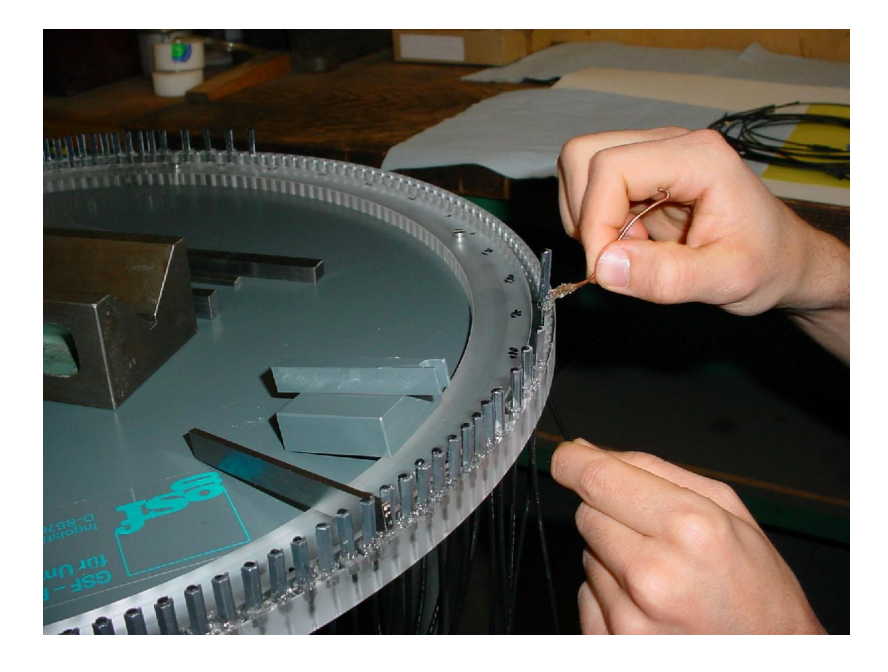


Figure 6. Detectors and shields in the process of being stuck to the PMMA basis.

### 2.3. Phantom Measurement

The device was mounted on a rotation desk and the whole assemble was placed in front of the X-ray source. The distance from the centre of the ring to the focal spot was 1 m. The focal spot has a size of 1.2 mm. The source is blended by a square slit and provides a maximum fan angle of 8 degrees. Therefore, the irradiated circular region in the centre of the device at the chosen distance to the focal spot has a radius of 7 cm. The whole set-up is shown in Fig. 7. The phantom chosen to fit this conditions was a halved pepper. Such a phantom has the advantage that it is organic tissue, it is empty in the centre, and also has a non-circular surface that should be easy to distinguish in the reconstruction of a slice.

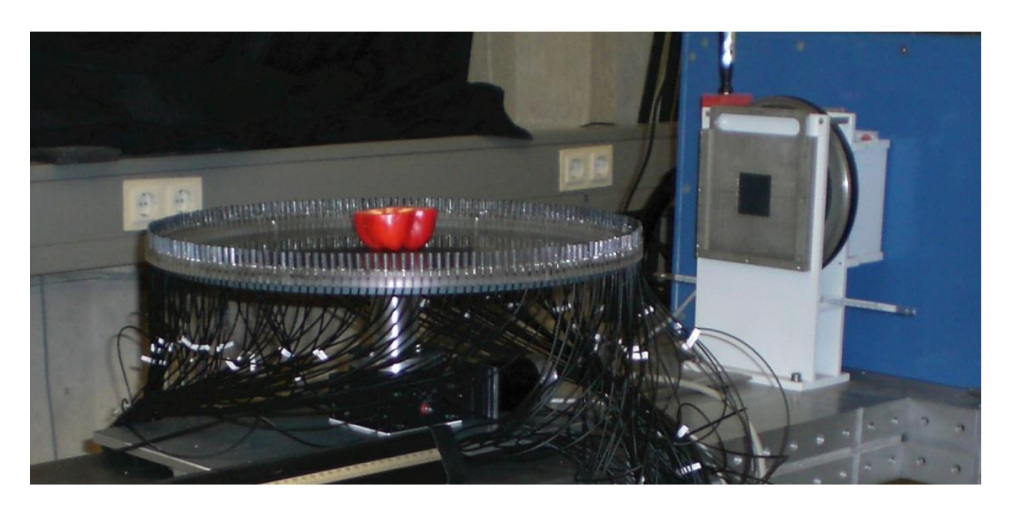


Figure 7. The whole device prepared to carry out the first measurement.

The schema of the parallel data acquired with our system is shown in Fig. 8. In the picture, the white regions between the rays (25 % of the total field of view) represent data that cannot be acquired with the present device, since the shields present a larger surface than the detectors.

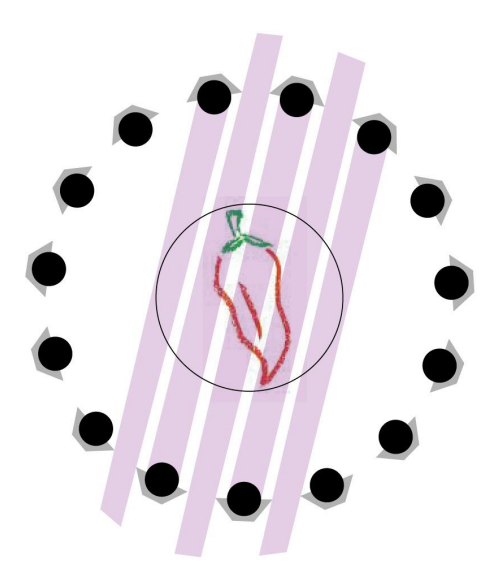


Figure 8. The parallel geometry for our device, in a simplified case of 15 detectors. For the depicted field of view, only 5 useful data are acquired.

The phantom was irradiated with photons of 100 kVp at a rate of 9.6 mA and keeping the filter of 4.05 mm Al. During the measurement, the detectors were set to acquire one sample of data per second. The data stored was automatically corrected by the factors  $F_i$  described above, which keeps a relation of proportionality among the detectors. The rotation table was programmed using LabVIEW 8.2 (National Instruments, Austin, Texas). In order to emulate a continuous rotation, it was set to rotate 3600 times in small steps of 0.1°. A delay of 2 seconds between the two consecutive rotations was included, in order to slow down the speed of rotation and increase the amount of photons received by the detectors. Hence there are 7200 samples for each detector during one whole cycle.

# 2.4. Data Analysis and Reconstruction

All samples were stored in a matrix of size 197 x 7200, where 197 is the number of detectors and 7200 is the total number of samples. All data cells below a given offset were set to zero. This operation shows clearly the predicted peaks that represent the moments during which the detectors receive radiation. The integration of these peaks separately produces the desired fan-data. Each peak integration represents one ray of the fan beam depicted in Fig. 9.

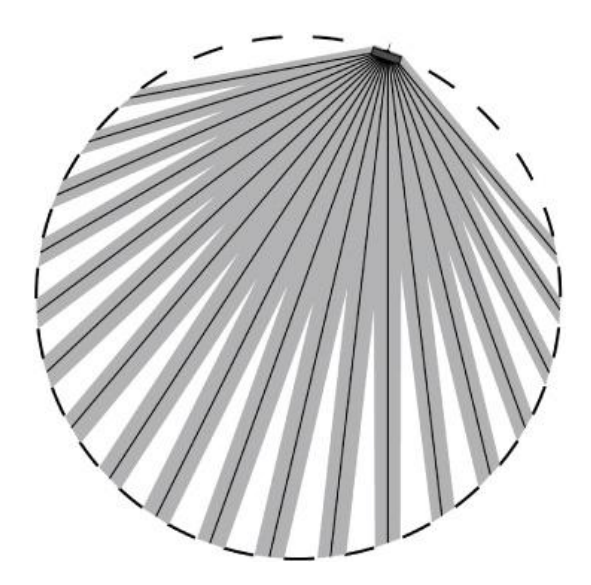


Figure 9.

The integrated data for one single detector corresponds to a fan beam. A simplified case of 27 detectors and 19 "rays" per detector is shown here.

The matrix I of integrated data was then normalised into the matrix N by

$$N_{i,j} = I_{i,j} \frac{m}{M_j},\tag{4}$$

where m is the maximum value of the vector M, whose  $j^{th}$  element  $M_j$  is the mean value of the non-zero data from detector j. this normalization helps to optimize the experimental calibration of the detectors a-posteriori.

The fan data need to be transformed into the parallel geometry. This is achieved by a simple reordering. Nevertheless, interpolation was necessary to fill 5% of the cells, which corrspond to failed detectors. The matrix of Radon data was then calculated by

$$R_{i,j} = \ln\left(\frac{\max(P_{i,j})}{P_{i,j}}\right),\tag{5}$$

and the reconstruction was carried out using the algorithm OPED.

#### 3. RESULTS

#### 3.1. Detector Calibration

The uncorrected response of the detectors is shown in Fig. 10 for the example of detector number 1.

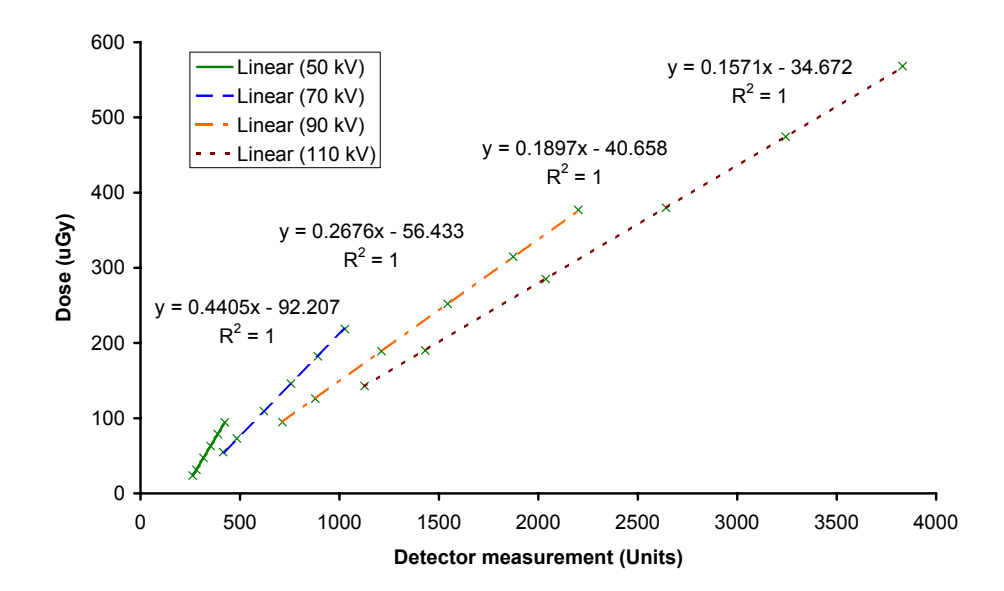


Figure 10. The linear response of detector number 1. The ordinates shown in the equations have no physical meaning. All curves show a common offset value (around 212 units for this detector).

The calibration and correction factors (obtained by Eqs. 1 to 3) are shown in Table 2 for the example of the first 5 detectors.

Detector No.	$S_{50}$	$S_{70}$	$S_{90}$	$S_{110}$	$F_{50}$	$F_{70}$	$F_{90}$	$F_{110}$	F
1	0.440	0.268	0.190	0.157	0.998	0.948	1.009	1.005	0.990
2	0.407	0.245	0.174	0.144	0.922	0.867	0.923	0.919	0.908
3	0.471	0.285	0.203	0.169	1.068	1.009	1.078	1.082	1.059
4	0.377	0.227	0.162	0.134	0.854	0.806	0.859	0.859	0.844
5	0.362	0.218	0.155	0.129	0.821	0.772	0.824	0.827	0.811
$\overline{S}_{ofall197}$	0.441	0.282	0.188	0.156					

**Table 2.** Calculation of the correction factor for the first 5 detectors

# 3.2. Phantom Reconstruction

The reconstruction carried out from data acquired using the new device is shown in Fig. 11. The original phantom is shown in Fig. 12 for comparison.

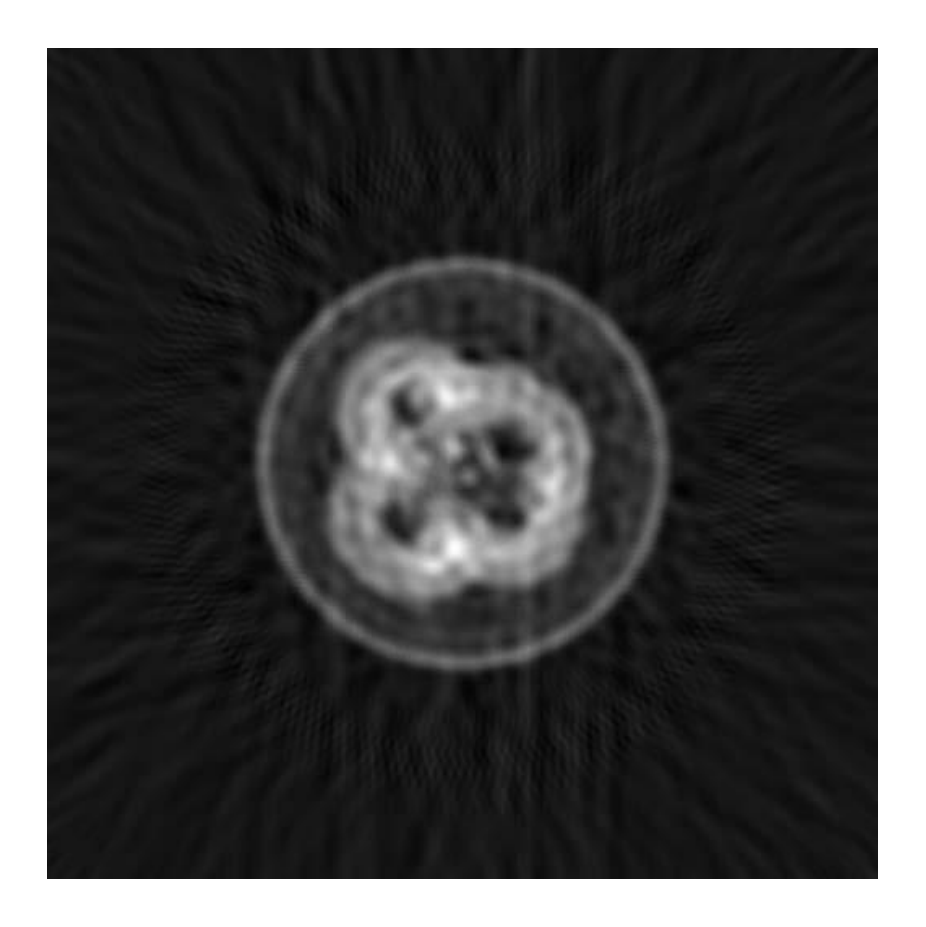


Figure 11. The reconstruction of a pepper slice. Observe the 4 lobules and the ring around it, caused by the lead shields.

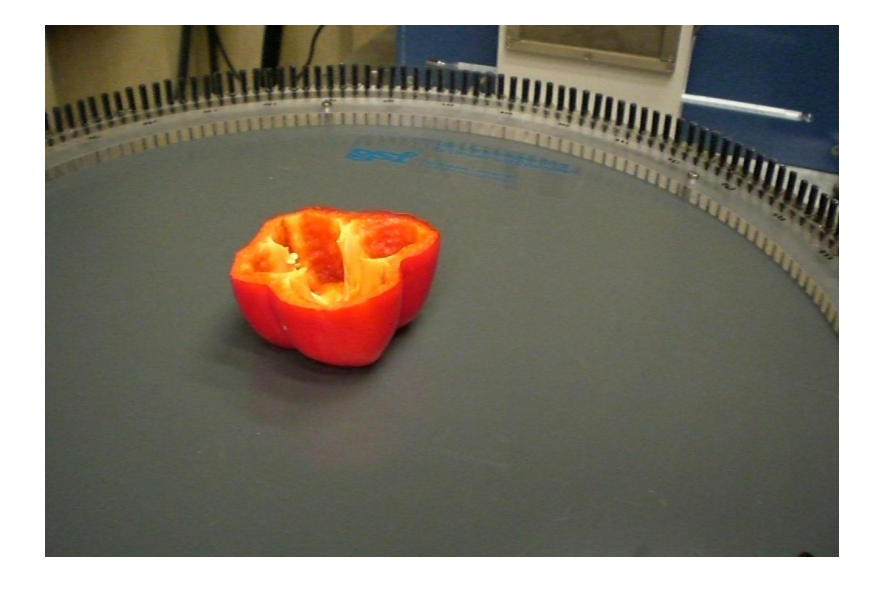


Figure 12. The pepper that was taken as phantom for the first measurement of the device, to compare with the reconstruction.

#### 4. DISCUSSION

#### 4.1. Calibration

The excellent linearity of the response should be noted, but also the fact that it is strongly dependent on the energy. The linearity of the crystal sensors is no longer valid only when the dose region corresponds to single photon counting, because of counting statistics. The background signal observed in Fig. 10 is probably due to residual currents in the photodiodes. It is different for every detector, but it can be easily subtracted during the measurements, before applying the correction factor.

The correction factors show a much lower dependence on the energy and are therefore more appropriate than the calibration factors for obtaining the data used for reconstructions. The estimation of the dose imparted to the phantom can be carried out by applying the calibration factors S for detectors that detect direct radiation (rays that do not pass through the phantom). For this provisional tests, the estimated dose to the phantom was in the range of  $100 \ mGy/s$  per unit area.

# 4.2. Prototype Device and Future Work

The experimental results are satisfactory for this simplified prototype. They demonstrated that the idea of new scanning device presented at last SPIE meeting is sound. Clearly various improvements can be carried out to optimise the quality of the reconstructions. An optimized version of this new scanner is expected to yield results promised by the theoretic prediction. What our simplified prototype lacks and how we plan to improve the system in the future, is listed below.

- 1. The outer detectors as proposed in the original idea were not included and therefore one half of the potential data from the phantom were not acquired, which means that the "dynamic" data promised by the theory are missing. We will use a flat-panel detector C-arm system for the next tests.
- 2. The thickness of the shields (5 mm) is larger than the size of the detectors (approx. 3 mm). As a result, 2/5 of the potential data are lost during measurements with this prototype device, which means that 2/5 of the "static" data promised by the theory are lost. Detector and shield shape will be modified in a future prototype.
- 3. The size of the detector's sensitive element (crystal) is about 1 mm. Despite great care, it was not possible to set them all in exactly the same plane manually. A future prototype design will contain slits that enable an exact positioning of detectors and shields.
- 4. The position of the focal spot source is only known approximately. So, it was not possible to find the correct position of the detector plane, on which the focal spot should lie. Hence, the reconstructed slice of the pepper was not exactly the central slice. We will map the radiation field to find this plane more accurately.
- 5. The fan angle is so small that the whole potential of the prototype could not be realized. In one parallel projection, there were only 17 useful data (see Fig. 8). This will be improved by using a different tube system.
- 6. Some detectors were not perfectly stuck to their holes in the PMMA or they were not properly attached to the fibre optic. As a result, some of them failed totally or partially during the measurement. Better mounting will be applied to avoid stress in the optical fibers.
- 7. Scattered radiation in the photodiodes introduced an energy dependence during calibrating and measuring. We will shield this radiation to the diodes.
- 8. The possibility of analysing the scattered radiation (during the time that no direct radiation is received by each single detector) has not been yet explored.
- 9. Measurements with standard phantoms will enable a rigorous image analysis in the future.

#### 5. CONCLUSION

A prototype of a new scanning device was built and used to test experimentally the theoretic prediction presented at last SPIE Medical Imaging Conference. The result serves as the starting point for a new CT scanner that will provide more efficient data acquisition and has the potential of dose reduction.

#### ACKNOWLEDGMENTS

The first author wishes to thank the people at the GSF-factory (especially Peter Streitenberger) for their engaged work and teaching, Raphaela Anselmann for her ideas during the calibration and Alexander Khegai for programming the rotation desk. The work of the first author was supported by a Helmholtz-DAAD Fellowship. His presence at this conference was financed by the GSF PhD Program.

#### REFERENCES

- 1. D. F. Regulla, H. Eder "Patient exposure in Medical X-ray imaging in Europe". *Radiat. Prot. Dosim.*, **114**, pp. 11-25, 2005.
- 2. H. H. Barrett and K. J. Myers Foundations of image science, John Wiley & Sons, Inc, Hoboken, 2004.
- 3. W. A. Kalender Computed Tomography, Publics Corporate Publishing, Erlangen, 2005.
- 4. F. Natterer *The mathematic of Computerized Tomography*, Reprint of the 1996 original. Classics in Applied Mathematics, 32. SIAM, Philadelphia, PA, 2001.
- 5. A. C. Kak and M. Slaney Principles of computerized tomographic imaging, New York: IEEE press; 1988.
- 6. O. Tischenko, Y. Xu and C. Hoeschen "A new scanning device in CT with dose reduction potential". *Proc. SPIE*, **2006**, 61422:893-899.
- 7. Y. Xu, "A direct approach for reconstruction of images from Radon projections", *Adv. in Applied Math* **2006**, 36:2388-420.
- 8. Y. Xu, O. Tischenko and C. Hoeschen "A new reconstruction algorithm for Radon Data". *Proc. SPIE*, **2006**, 6142:791-798.